Formation Kinetics of the Self-organized III-V-based Nanostructures Grown by Droplet Epitaxy

Ákos Nemcsics

Institute for Microelectronics and Technology, Óbuda University
Tavaszmező u. 17, H-1084 Budapest, Hungary; and
Research Institute for Technical Physics and Materials Science, Hungarian
Academy of Sciences, P.O.Box 49, H-1525 Budapest, Hungary
e-mail: nemcsics.akos@kvk.uni-obuda.hu

Abstract: In this work, we discuss the evolution of self-assembled III-V-based nanostructures. These nanostructures were prepared from Ga droplets during a crystallization process using a droplet epitaxy technique. Different nanostructures such as quantum dots, quantum rings, double quantum rings, and nano holes were formed from Ga droplets on a (001)-oriented AlGaAs surface, but at different substrate temperatures and various arsenic background pressures. We give a qualitative description of the elemental processes for the formation of all of these nanostructures. Our description is based on the size dependence of the key material properties (solubility, tension, etc.).

Keywords: GaAs; droplet epitaxy; quantum dot; quantum ring; nano hole

1   Introduction

Low dimensional structures grown by molecular beam epitaxy (MBE) revolutionized electronic devices, both in terms of their potential and their efficiency. Nowadays, the growth of self-organized nanostructures is thoroughly investigated for basic physics and device applications. It is very important to understand their growth kinetics and to know their shape. The most widespread technique is based on the lattice mismatched Stranski-Krastanov growth mode [1, 2]. An example is the MBE growth of InAs quantum dots (QDs) driven by strain between the deposited InAs and the substrate. For a long time, this strain-induced method was the only known process for zero dimensional structure production.

A droplet epitaxial technique based on Koguchi's discoveries has evolved, giving greater opportunities for the development of the self-organizing nanostructures [3, 4]. In this method, the lattice-mismatch loses its significance and it becomes

possible to create QDs [5-9], quantum rings (QRs) [10-12], double quantum rings (DQRs) [13, 14], as well as nano holes (NHs) [15-17] (see Fig. 1). The electronic structure of these nano-objects depends very much on their shape. The droplet epitaxial process roughly consists of the following steps: first, metal (e.g. Ga) droplets are generated on the surface in the Volmer-Weber-like growth mode. After that, crystallization of the droplets occurs together with their chemical transformation, e.g. GaAs QDs under arsenic pressure. In order to control the process it is necessary to understand the kinetics of the growth processes, but no theoretical description is available yet of the underlying growth mechanism. In this paper, we study the formation and properties of GaAs nanostructures grown on AlGaAs (001) substrate as a function of the applied technology.
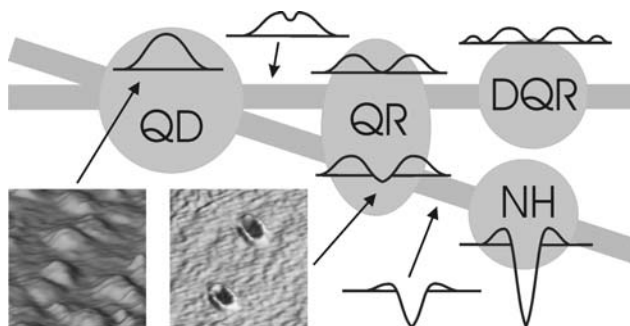

Figure 1

Overview of the III-V-based dropletepitaxially grown nanostructures such as quantum dots (QDs), quantum rings (QRs), double quantum rings (DQRs) and nano holes (NHs)

2   Experimental Preliminaries

The growth experiments were made in a solid source MBE system. The evolution of the growth front was monitored in the [1$\underline{1}$0] direction with reflection high-energy electron diffraction (RHEED). After the growth, the QDs were investigated using atomic force microscopy (AFM) in tapping mode. Droplet epitaxial GaAs QDs were formed on the AlGaAs (001) surface (with Al content of $x = 0.3$).

The main steps of the droplet epitaxial process of QDs were as follows: Following the preparation of $Al_xGa_{1-x}As$ surface, the samples were cooled to 200 and 250 °C, Ga was deposited first (the surface coverage Θ=3.75 mono layer (ML)) with the flux of 0.15 and 0.025 ML/s without the arsenic flux, respectively (sample type a and b). After a few seconds' waiting time, an annealing step was performed at 350 °C under 6.7×10^{-5} mbar arsenic pressure. A detailed experimental description is published elsewhere [18].

In the case of sample type *c* (droplet-epitaxial QRs), after the preparation of the AlGaAs layer, the sample was cooled to 300 °C, and θ=3.75 ML Ga was deposited with the flux of 0.75 ML/s without arsenic flux. After Ga deposition, 60 seconds' annealing (300 ºC), under 5.3×10^{-6} mbar arsenic pressure, was applied. A detailed description of the growth parameter is published elsewhere [19].

A further five types of nanostructures (sample types *d* - *h*)were also prepared. The technological parameters are given as follows: The solution process was investigated in two variations (sample types *d* and *e*). NHs (sample type *d*) were generated at 570 °C in AlGaAs surface applying 6.4 ML Ga [16]. In this case, the AFM measurement shows NHs and very large clusters [16]. Other types of NHs (sample type *e*) were prepared similarly, but the Ga coverage was different (3.2 ML) [15, 16]. Here, the AFM picture shows deep NHs surrounded by ring-like bulge formations and shallow NHs, with plane rims (without any bulge) [15, 16].

The crystallization process is investigated in three variations of samples (sample types *f* - *h*). The first nanostructure is a very fast-crystallized QD (sample type *f*). The crystallization of the Ga droplet occurs during the high arsenic supply (3.3×10^{-4} mbar) at 150 °C [8]. The elementary map of transmission electron microscopy (TEM) shows that the QD had Ga inclusons [8]. The second type of samples (type g) is crystalized at 2.7×10^{-6} mbar arsenic pressure at low temperature (200 °C) [13]. In this way, we received DQR [13]. The last sample (type *h*) is crystallized at about the same arsenic background (1.5×10^{-6} mbar) but at a high temperature (500 °C) [17]. The middle of the structure is surrounded by single ring-like bulge formations [17]. For the detailed technological parameters of the above samples see the given references.

3   Discussion

3.1   Formation Kinetics of Quantum Dots

The formation of the QD structures was in-situ monitored by RHEED. Firstly, Ga droplets were formed on an AlGaAs (001) surface. As the second step, the droplets were transformed into QDs under an arsenic environment. In order to investigate of droplet formation in one occasion, the preparation procedure of QDs was interrupted before the crystallization step. This particular sample was quenched and inspected by AFM immediately after the Ga droplets were formed. This AFM image was compared to another sample, on which the Ga droplets, formed under identical conditions, were reacted with As in the crystallization step. The density and the size of QDs were found to be identical to te Ga droplets. Because of the grazing incidence angle, the RHEED pattern is characteristic for the nano structure (see Fig. 2/A). The Ga clusters formed on the surface are liquid

aggregates; this status is proven by the RHEED picture as well as by the shape of the clusters. The sharp RHEED streaks characteristic of the AlGaAs (001) surface vanished after Ga deposition and the streaky RHEED picture becomes diffused because of the electron beam crossing the liquid aggregate. The RHEED temporal patterns of the QD formation are shown in middle part of Fig. 2/B-E. As mentioned before, the Ga clusters before crystallization are investigated with AFM working in tapping mode. The original shape of the droplets is conserved during the AFM measurement due to the residual adsorbate on the droplet surface, which exists also under 10^{-10} mbar [20-22]. The shape of these clusters follows the law of the surface and interface energy minimization (see later) [23-29].
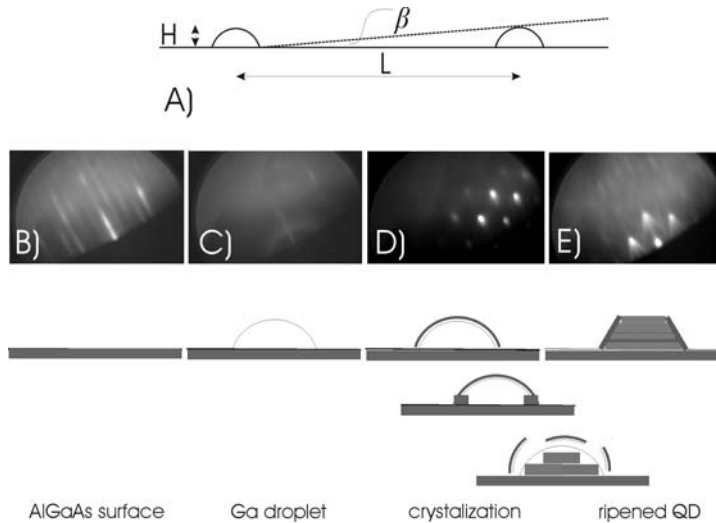

Figure 2

(A): The RHEED geometry on the surface. At N_1=1.2н10^{10} cm^{-2} and N_2=4.4н10^8 cm^{-2}, the average height (H) of the droplet and the characteristic average distance (L) between these nanostructures are H_1=7 nm, H_2=32 nm and L_1=90 nm, L_2=477 nm, respectively. The RHEED pattern is characteristic to the nano-structures, because the β_1=4º and β_2=3.8º are larger than the incidence angle (about 2º) of the electron beam; (B)-(E): The RHEED pattern and the corresponding sketched stage of the QD evolution

On the initial surface (Fig. 2/B), droplets with rounded shape are formed (Fig. 2/C). After this, a monocrystalline outer shell develops (due to the adsorbate effect, mentioned before). This is verified by the dotted RHEED pattern (Fig. 2/D). Thirdly, the crystallization process occurs, showing signs of the crystallographic planes inside the QD (Fig. 2/E). Here, the timing of the process of the RHEED sequence and the duration of each RHEED stages are also relevant. For many seconds, the dotted stage (Fig. 2/D) remains unchanged, but after that, the chevron tails develop relatively quickly (Fig. 2/E). The developing planes correspond to crystalline facets, verified by chevrons on the RHEED picture [18]. The evolution of the structure is sketched in the lower part of Fig. 2.
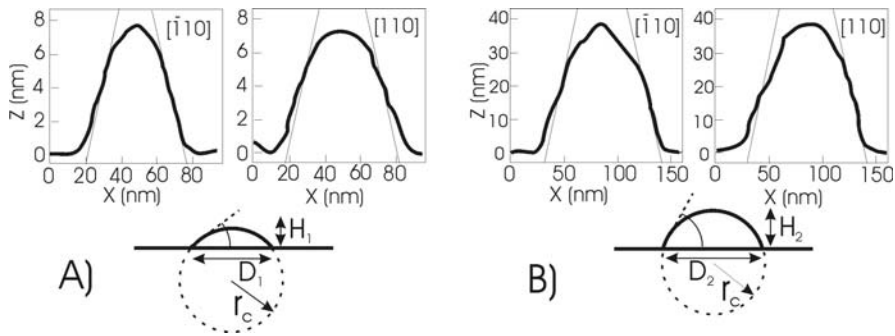
Figure 3

AFM line scans of single QDs along [1$\underline{1}$0] and [110] azimuth. (A) and (B) show typical line scans and the sketched droplets with parameters (high H, sole diameter D, critical radius r_c; the explanation see later) of the sample type a and b, respectively

In our earlier studies, the grown QDs can be classified two groups by their size and shape [18] (see Fig. 3). Here, we will show that shape of the QD depends on the shape of the droplet. Moreover, the size and the shape of the initial droplet is determined by the process of Ostwald ripening [30-36]. Furthermore, the shape of the droplets is also determined by the surface tension in the liquid aggregate and by the wetting properties at the interface.

The contact angle (the angle at which the tangent at a liquid/vapour interface meets the solid surface, called the three-phase line (TPL)) is characteristic of the surface. In practice, droplets (with mm size) are used for surface characterization [37-39]. Surface tension is caused by the intermolecular forces on surface of the liquid [40]. This tension is an effect within the surface layer of a liquid that causes that layer to behave like an elastic sheet with a thickness of approximately 10 nm [41]. Inside of this very thin sheet, the forces are independent of the length of the sheet. (Therefore, the behaviour of these forces differ fundamentally from the force in an elastic membrane.) At macroscopic scale, the interaction between forces across the three interfaces are independent of the dimension of the droplet, and therefore they can be used for surface characterization [38, 39].

These forces in the surface sheet are independent of the area and only depend on the thickness, therefore, of the number of interacting molecules in the unit area. (For example, in a free-standing membrane, the force is doubled; therefore, we must double the thickness as well in the calculations.) In reality, the dimensions of the droplet are much larger than the thickness of the surface sheet. If the dimension of the droplet decreases to the nano range, and the size becomes comparable with the dimension of the thickness of surface sheet (approx. 10 nm), then the shape of the droplet (the contact angle) changes. The tension also depends on the temperature. It decreases with increasing temperature [41], and it also decreases with increasing ambient pressure [42]. The surface wettability (and also the contact angle) depends very strongly on the properties of the substrate surface.

Molten Ga droplets were investigated on a pure GaAs substrate in a hydrogen atmosphere [43]. At 852 °C, typical to liquid phase epitaxy, the contact angle is 28°. It was found that the temperature coefficient is 3.6°/100 °C [43]. At 250 and 200 °C the contact angles are thought to be around 50° and somewhat larger, respectively. In our case, the droplets are in a vacuum (pressure conditions are different); therefore, the contact angle can be expected to be somewhat different from the calculated one. Furthermore, it was found that on the AlGaAs substrate, the contact angle increases with the increased Al content [43]. Our substrate has x=0.3 Al content: therefore, the estimated contact angle is few degrees larger than 50°. It is evident that larger QDs originate from larger droplets (and smaller ones from smaller). The relation between density and size of QDs is governed by Ostwald ripening [30-36].

We will show later that the facet angle of the QDs depends on the contact angle of the initial droplet and, furthermore, that it is realistic to suppose that the larger droplet – similarly to the macroscopic case – has a contact angle slightly larger than 50°. It will be verified that the contact angle of the lower droplet is around 25°.

In our previous experiments, we found two distinct regimes for the QDs shapes (see Fig. 3.). When the Ga flux is low (F=0.025 ML/s, T=250 °C), the probability of the nucleation is low. With decreasing adatoms (and increasing temperature), the Ga atoms attach themselves to existing clusters rather than nucleate new ones. Therefore in this case we have larger QDs (average height n_1=32 nm, average base width d_1=110 nm) with lower density (n_1=4.4×10⁸ cm⁻²), and with a facet angle of about 55°. We observed in the experiment that the size and shape of the QDs did not differ greatly from each other. According to the experiment, it is probable that the contact angle is likely to be found at around 55° (somewhat larger than 50°). For higher Ga flux (F=0.19 ML/s, T=200 °C), the probability of nucleation is high. We observed smaller droplets (h_2=7 nm, d_2=60 nm) with higher density (n_2=1.2×10¹⁰ cm⁻²). We also found a fundamental difference in the shapes of the QDs in two different growth regimes (sample types a and b, respectively). In the latter case, the side angle of the QDs was found to be 25° (where the contact angle of the droplets was also about 25°.) This proves that the quantity of the deposited Ga atoms is in correlation with the volume of the droplet, according to the results on the QD facets, shown previously [18].

Let us assume that the shape of the droplets is a segment of a sphere (see. Fig. 4/A), where R is radius of the sphere, D is a cord as shown in the figure, α is the contact angle, H is the height of the droplet, V is the volume of the droplet and n is the density of the droplets. The radius of the curvature can be calculated from the equation: $R=D/2sin\alpha$ or $R=H/(1-cos\alpha)$. For smaller droplets, the calculated radius from both formulae is the same, R = 68 nm and the contact angle is 26°. For the larger droplets, the radius – according to former calculations – is 71 nm with a contact angle 57°. The droplet volume can be calculated either from the spherical volume formula: $V=\pi h^2(R-H/3)$ or from the dot density: $V=(\Theta-1)/n$. The number of

Ga atoms in the droplets can be estimated by using both formulae. The atomic radius of Ga is 0.13 nm [44]. This corresponds closely to the half of the minimum bond length. The calculated atoms in the droplet are in order of one million. The atomic interaction in a large cluster (the atomic number $\geq 10^6$) is similar to in bulk material [45]. It is also known that the surface tension is caused by the attraction between the short radius intermolecular forces. This tension is a surface effect which behaves like a very thin (in order of the nm) elastic sheet [41].
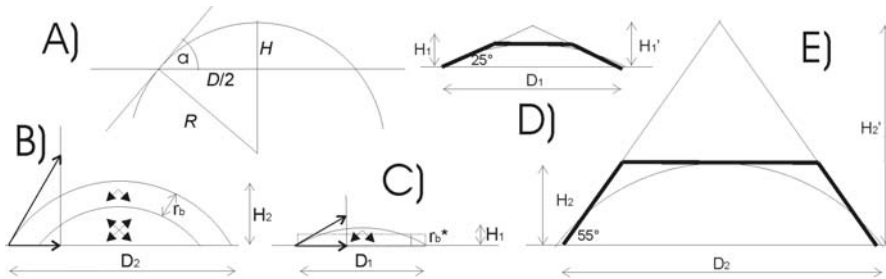

Figure 4

(A): schematic diagram of the droplet for the calculation of curvature; (B) and (C): Illustration of the effect of the contact angle and the size: for large droplet, the size is large enough; for a small droplet, the droplet size and the surface sheet dimensions are comparable. (D) and (E): Formation of truncated pyramid-like QDs (see text)

Now we can estimate the contact angle. The surface tension depends on the thickness of the surface sheet (see doubling effect). The contact angle dependence on the surface sheet can be seen in Fig. 4/B. In our calculation, we used a numerical value of r_b=10 nm [41]. For the big droplets, the volume is large enough for the surface sheet to be similar to that of the macroscopic case. The contact angle is over 50°, as shown earlier. This contact angle corresponds roughly to the side angle of the large QDs. For a small droplet, however, the situation is quite different. Here, the height of the droplet is comparable (even below) to the thickness of the surface sheet and the surface tension is proportional to the thickness of the sheet. The effective sheet thickness (r_{beff} calculated from the volume of the sheet) is approx. 6 nm, where the effective or average thickness is defined as the volume of the sphere segment normalized to the surface area of the interface between the droplet and the substrate (see Fig. 4/C). From here, the contact angle is around 30°. The contact angle corresponds roughly to the side angle of the small QD. The follow up phase in the QD production is the crystallization. The kinetics of the crystallization process is not yet known. We know that when the dotted diffraction picture of the transmission RHEED develops very quickly, it characterises the monocrystalline state. As we said before, the monocrystalline shell develops on the droplet surface due to the adsorbate effect [20]. The lateral formation of crystal surface is determined by the orientation of the new external surface element of the crystal in a defined crystal position of the melt surface adjacent to the TPL. The crystal surface coincides

approximately to the tangent to the phase boundary at a point on the TPL [46]. That is, the crystal facet of the QD corresponds to approximately the contact angle of the droplets. For a small droplet (a contact angle of less than 30°) the grown side-facets are around 25° after crystallization, corresponding approx. to (113) or (137) crystal planes (see Fig. 4/D). For a large droplet (a contact angle of more than 50°) the grown side-facet is around 55° after crystallization, corresponding to (111) crystal plane. The temporal evolution of the crystallization breaks up at one point, because the Ga atoms are all used up from the droplet; therefore, the QDs take up a truncated pyramid shape (see Fig. 4/E).

The TPL at the droplet edge initializes the crystallization. A number of crystallization seeds form at the same time in a number of equivalent places. The dotted RHEED picture indicates that all of the seeds are coherent oriented, so they have a monocrystalline character. The crystallization may occur uniformly distributed amongst these equivalent places. The liquid phase has short-range order lines and the droplet sizes are falling in this range. The liquid phase in the droplet can be described as a crystalline-like structure [45, 47]. We can conclude that the coalescence of the simultaneously appearing nucleation centers grow into a monocrystalline form and not into the usual polycrystalline form. When the surface area minimization takes place (between the droplet state and QD state), the crystal planes of the QDs must come near to the tangential planes of droplet [46]. If we assume a simultaneous crystallization process, than we come very close to the already described shapes for the QDs. The crystalized QDs are truncated, setting the sole width, the facet angle, the height and also the shape of the droplets.

The effect of the adsorbate and its segregation can strongly alter or even block the crystal growth locally and can lead to the rounding of crystal shapes [21, 22]. This effect explains the existence of the pure dotted RHEED picture during crystallization. On the RHEED picture, chevron tails form relatively quickly in the later stage of crystallization. This behaviour explains the phenomenon that the growing crystal facets explode the outer adsorbing shell, and instead of round crystal surface, in the result is a sharp crystal facet. The resulting nanocrystal corresponds to the Wulf construction [23-29].

3.2   Formation Kinetics of Quantum Rings

The QR evolution was tracked in-situ manner with the RHEED technique. In the initial stage, the perfect crystalline AlGaAs (001) surface causes sharp RHEED streaks. After the deposition of Ga, this picture becomes diffuse, due to the amorphous nature of the phase present on the surface. The annealing phase begins after the offering of an arsenic component with the pressure of 4×10^{-6} Torr, while the substrate temperature is 300 °C (sample type *c*). After the introduction of arsenic, some time is needed for the formation of the characteristic sharp pattern, representative of the crystalline structure (see Fig. 5/A). This shows that the liquid state on the surface stays for longer time and the material transport processes in it

propagate the formation of the QRs. This is different to the QD formations, where the RHEED pattern characteristic of the crystalline phase coincides with the opening of the arsenic cell [48]. The QR structures were ex-situ investigated with AFM. The perspective AFM image and the top view with line scans are shown in Figs. 5/B and C, respectively. The dimensions of the QRs were determined from individual line scans. Two typical adjacent AFM line scans are shown in the right side of Fig. 5/C. The density of the QRs was determined from the AFM pictures as 1.5×10^9 cm^{-2}. It is observable that the middle of the QRs is located deeper than the original surface level. It can be shown from the AFM measurement that the shape and size of the QRs are near uniform, but we can observe small deviations from the average size and form. It has been observed frequently that the smaller diameter QRs have deeper cavities in the centre and opposite; that is, the larger diameter QRs have shallower cavities in the middle. (In the figures, the smaller and larger objects are labelled with "S" and "L", respectively.) Fig 5/C shows that the QRs are a little elongated (see top view), the phenomenon of which is based on the different binding properties in [110] and [1$\underline{1}$0] directions. Here, the phenomenon is neglected, because it does not influence our order of ideas, since the larger QR is larger in both lateral directions, and the smaller one is the opposite.
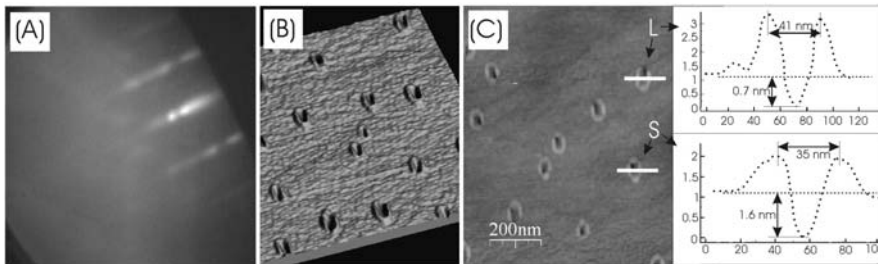

Figure 5
(A): The RHEED pattern of the QR structures; (B) Perspective AFM picture of sample surface with QRs; (C):Top view of the AFM image ith line scans (see text)

This interesting contradictory property of the QR aspect ratio can be explained as follows. During the deposition of the Ga, droplets form on the AlGaAs surface. It can be presumed that the larger droplets lead to the development of rings of larger diameter, and the smaller droplets to smaller rings. The intersection of the crystal surface with the droplet edge is the three-phase-line, which serves as initial place of crystallization [49, 50]. The three-phase-line of larger diameter attaches to the larger droplet and the one of smaller diameter attaches to the smaller droplet. It is known from the liquid phase epitaxy that thermal etching takes place at the Ga melt and AlGaAs surface [51]. This phenomenon was confirmed via analytical transmission electron microscopy in the case of droplet epitaxy [52]. The Ga melting can solve the arsenide molecules (e.g. GaAs). These arsenide molecules originate partly from the thermal etching of the crystal surface and partly from the

reaction of the external arsenic atoms. (When a Ga atom of the droplet meets an arsenic atom from the environment, they form a GaAs molecule.) These molecules causing thermal movement in the droplet can reach the three-phase-line, where the crystallization takes place. During the process of this solidification, a material transport takes place from the middle to the edge of the nanostructure. Thus, a circular crystalline phase is formed at the droplet edge. During the solidification process, the amount of Ga atoms in the droplets decreases, so the droplet size decreases, as well. The proposed kinetics of the formation is sketched in Fig. 6. During thermal etching, not only arsenic and gallium but also aluminium leaves from the AlGaAs surface, and is built into the lattice matched crystalline pair, which was shown earlier for QD [52]. We can suppose that the situation for QR is similar.
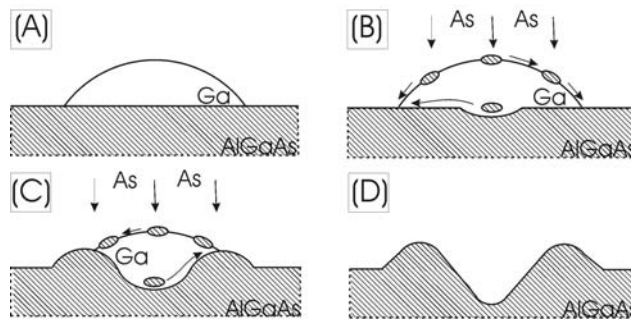

Figure 6

(A)-(D): Different states of the evolution of the droplet-epitaxial QR (see text)

It is known that the melting point decreases with the reduction in the particle size [53, 54]. Fig. 7/A shows the normalized melting curve for a metal vs. diameter of the particle. The figure shows that if the size is less than 50 nm, then the melting point depends very strongly on the size. In the nano range, the melting point is determined more strongly by the size than by bulk properties. The experimental melting curves for near spherical metal nano particles exhibit similarly shaped curves. For our case, this curve is gives direction for qualitative consideration. It means that the melting point in the larger and smaller Ga droplet can differ strongly. Fig. 7/B shows the solubility curves for different particle sizes. The figure shows that under the same temperature, the larger droplet has a lower saturating concentration and the smaller droplet has a higher one [55]. This means that the crystallization in the larger droplet will take place earlier that at a smaller arsenide concentration. The smaller droplet will crystallize later only at higher arsenide concentrations.

The temporal evaluation of the smaller and larger QR is shown in Fig. 7/C. In other words, in the larger droplets, the probability of the formation of crystallization seeds is higher; therefore, the crystallization takes place earlier, so less time is spent on material transportation, causing the development of the hole

in the middle. In the smaller droplets this probability is smaller; crystallization starts later, so more time is spent on deepening the middle of the ring. This process is influenced by other factors as well. As the melting temperature of the nanostructure drops with its diminishing size, a smaller droplet will stay longer in liquid state at the same temperature; therefore, more time can be spent on the central cavity formation. This diameter versus central depth relationship can only be considered on statistical grounds. The likely reason is that the forming process depends not only on the size of the droplets, but also on the arsenic molecules, whose presence is independent of the size of the droplet. Homogeneity of the distribution and the size of the nanostructures are quite uniform. We also monitored some deviations from the rule.
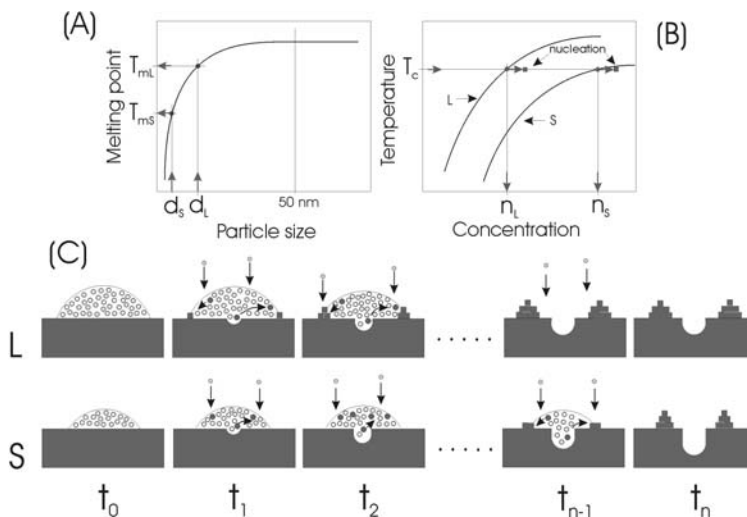

Figure 7
(A) The melting point dependence vs. particle diameter. If the size less than 50 nm then the dependence is very strong. (B): The solubility for different droplet sizes; (C): Temporal evolution of the QR for larg and for small droplet size

3.3   Formation Kinetics of Special Shaped Quantum Structures

Here we deal with the formation kinetics of particular shaped droplet epitaxially grown nanostructures. As is widely known, the properties in the nano region differ from the bulk properties. Generally, the nano-properties are unknown and only the tendency of the change is established, relative to the bulk properties. Usually the starting and the end states are known. The explanation of the final process comes from the coherent explanations of the component processes. These process explanations are coherent and consistent only when they describe the growth of a large number of different kinds of nano-structures. Only then do they become consistent.
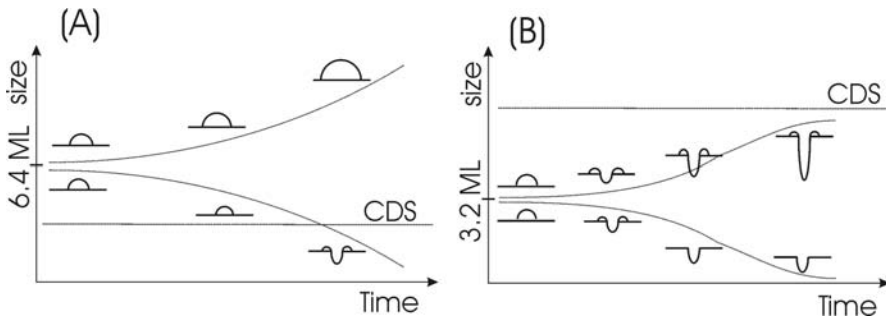
Figure 8
(A): Explanation of the temporal diferentiation and solution process in case of large amount of deposited Ga (6.4 ML), (B) Explanation of this process at small Ga amount (3.2 ML) (see text)

After the deposition of Ga, part of the deposited Ga will combine with the surface arsenic atoms and the rest will form droplets. In order to form droplets at this temperature, the Ga atoms must migrate (process *i*) on the GaAs and the Ga surfaces. It is well known that with diminishing size the melting temperature drops and saturation concentration increases. This describes our present Ga droplets well (process *ii*) (this is the dominant process in cases of a complete lack of or only small quantities of arsenic). It is also well known that the crystallization starts at the three-phase-line when the conditions became favourable. In our case, this starts in the line of the rim of the droplet (process *iii*). It is noted that the excess arsenic incorporates into the GaAs epitaxy when the temperature is low (about 300 °C or lower), creating stress in the lattice. (In presence of a larger quantity of arsenic, these are the dominant processes).

Process (*i*) allows for the phenomenon called Ostwald ripening [30-36]. At the same time, process (*ii*) causes the differentiation between QD-s, QR-s and NH-s. Due to this process, at the same temperature and during the same time, the hole which originates under the smaller droplets is deeper than that which is under the larger droplets (Fig. 8). (That is supposing the time duration is not so long asto run out of the material from the smaller droplets.) These findings are proved by the two experiments, where the deposited Ga quantity was 6.4 ML (Fig. 8/A) and 3.2 ML (Fig. 8/B), respectively. At a given temperature there is a critical droplet size (CDS) under which the solution begins. After the Ga deposition, droplets form, followed by the growth of the larger droplets at the expense of the smaller ones. When the critical size is reached, the substrate solution by the droplet begins. We start by investigating the case of Ga 6.4 ML [16]. During the experiment, the formation of small NH-s and large QD-s can be observed (sample type *d*) [16]. We can follow the process on Fig. 8/A, where a large quantity of Ga is deposited. The sizes of the droplets formed are above the CDS. After the deposition, the differentiation of the droplets begins. The smaller droplets reach critical size and start solving the substrate. This state is frozen via opening the arsenic cell.
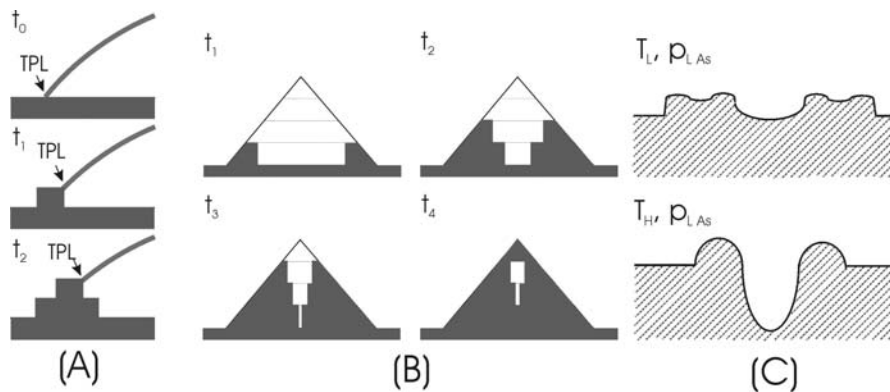
Figure 9

(A): Explanation of the crystal seed formation at the droplet rim; (B): Explanation of the formation of
Ga inclusion inside of the QD; (C): upper and lower part show cross section of a DQR and NH,
respectively

The second case is when the deposited Ga is 3.2 ML [15, 16]. Here, we can observe shallow NHs, with plane rims (without any bulge) and deep NHs surrounded by ring-like bulge formations (sample type *e*) [15, 17]. The explanation is given in Fig. 8/B. In this case, the quantity of the deposited Ga is small. The formed droplets are under the CDS; therefore the solution starts under the droplets. Under the small droplets the solution is faster, but the material is used up in a short time. The reduction in material is due first to the solution and second to the material's migration towards the larger droplets. After a short time, at the smaller droplets the solution stops, whilst it carries on further under the larger ones. The larger droplets will not be spent, and therefore the surrounding ring will freeze after the opening of the arsenic cell.

Due to the third process, the crystallization originates at the rim of the droplets. At a lower temperature the excess arsenic is incorporated into the lattice. The interstitial arsenic migrates towards the inside of the structure, reducing the lattice stress. A new interface is created in the inner and upper regions of the crystal centres. The growth of these centres propagate in those directions (Fig. 9/A). The arsenic is fed from the outer surface of the structure. It was observed that when the arsenic quantity was large, the QD had Ga inclusions (sample type *f*) [8]. Their origin is explained above. The growth in height is similar to that of the basic circle; so the speed of growth in height is a linear function. The speed of growth towards the inner regions accelerates because, assuming constant arsenic absorbing surface, the concentric area diminishes with the reduced radius going towards the centre (Fig. 9/B). The presence of the excess arsenic at a lower temperature is the explanation for the formation of the DQRs. The migration and the crystallization of the Ga would result in the creation of a larger ring (upper part of Fig. 9/C, sample (type *g*)) [13]. Instead, in addition to the original ring we end

up with a second ring, and this limiting effect on the size of the area is the result of the elimination of the lattice stress. The creation of DQRs can only be observed at a lower temperature. At a higher temperature DQRs cannot be created because the arsenic is not incorporated into the lattice, which causes the stress in the lattice (lower part of Fig. 9/C, sample (type *h*)) [17].

Conclusions

Here, we described the formation of several droplet-epitaxial nano-objects. In the first part, two separate regimes are investigated for the strain-free GaAs QD shape, using Ga droplet epitaxy for the growth. On one hand, the accurate facet angles are determined by the crystalline planes; on the other, the coarse angles of inclination of the QDs are determined by the contact angles of the droplets. A spherical approach was used for the describing shape of droplets. The volume and the shape were controlled with the data from AFM. The resulting contact angle was correlated with the surface tension dependence on sheet thickness (size effect). The shape of the QDs depends on the droplet volume. Larger QDs have a strongly truncated pyramid-like shape with side-facets 55°. Smaller QDs have a slightly truncated pyramid-like form with side-facets 25°, verified by AFM results. The correlation between the size and shape of the droplets and the QDs was also investigated. We showed that the shape of the droplet in the nano range depends on its size. We also showed that the nano structure during crystallization has a monocrystalline character and a rounded outer surface due to the effect of adsorbate. This is in an agreement with the dotted RHEED picture. The chevron tails which form in the late stage of crystallization process can be explained by a break in the adsorbate shell of the structure. The results correspond with the Ostwald ripening and with the Wulf construction.

In the second part of this paper we attempt to explain the kinetics of the epitaxial growth of QRs. What triggered the investigation was the realization of one peculiar characteristic feature of QRs during experimentation. That is, often the middle of the larger rings is shallower than that of the smaller ones. The arsenic molecules arrive to the surface in random distribution and therefore the above phenomena is superimposed on random noise. The cause of the phenomenon is the dependence of the melting point and the saturation concentration on the size of the nanostructure in this size range. We are confident that with this interpretation, we approach the correct explanation of the kinetics of the droplet epitaxy.

In the last part, we explain the formation kinetics of a few special-shaped nano-structures. One of them is the QD with Ga inclusion. The explanation is based on the excess arsenic content in the grown crystal at low temperature. Temporal differentiation was observed during the growth of NHs. We introduced the CDS to explain this phenomenon.

Acknowledgement

References

[1]   D. Leonard, M. Krisnamorthy, C. M. Reaves, S. P. Denbaas, P. M. Petroff; Appl. Phys. Lett. 63 (1993) 3203

[2]   V. Bessler-Hill, S. Varma, A. Lorke, B. Z. Nosho, P. M. Petroff; Phys. Rev. Lett. 74 (1995) 3209

[3]   N. Koguchi, S. Takahashi, T. J. Chikyow; J. Cryst. Growth 111 (1991)

[4]   N. Koguchi, K. Ishige; Jpn. J. Appl. Phys. 32 (1993) 2052

[5]   T. Mano, K. Watanabe, S. Tsukamoto, H. Fujikoa, M. Oshima, N. Koguchi; Jpn. J. Appl. Phys. 38 (1999) L1009

[6]   J. M. Lee, D. H. Kim, H. Hong, J. C. Woo, S. J. Park; J. Cryst. Growth 212 (2000) 67

[7]   Ch. Heyn, A. Stemmann, A. Schramm, H. Welsch, W. Hansen, Á. Nemcsics; Appl. Phys. Lett. 90 (2007) 203105

[8]   T. Mano, K. Mitsuishi, Y. Nakayama, T. Noda, K. Sakoda; Appl. Surf. Sci. 254 (2008) 7770

[9]   Á. Nemcsics, L. Tóth, L. Dobos, Ch Heyn, A. Stemmann, A. Schramm, H. Welsch, W. Hansen; Superlatt. Microstr. 48 (2010) 351

[10]   T. Mano, N. Koguchi; J. Cryst. Growth 278 (2005) 108

[11]   T. Kuroda, T. Mano, T. Ochiai, S. Sanguinetti, K. Sakoda, G. Kido, N. Koguchi; Phys. Rev. B 72 (2005) 205301

[12]   Á. Nemcsics, Ch. Heyn, A. Stemmann, A. Schramm, H. Welsch, W. Hansen; Mat. Sci. Eng. B 165 (2009) 118

[13]   S. Sanguinetti, M. Abbarchi, A. Vinattieri, M. Zamfirescu, M. Gurioli, T. Mano, T. Kuroda, N. Koguchi; Phys. Rev. B 77 (2008) 125404

[14]   T. Kuroda, T. Mano, T. Ochiai, S. Sanguinetti, T. Noda, K. Kuroda, K. Sakoda, G. Kido, N. Koguchi; Physica E 32 (2006) 46

[15]   Ch. Heyn, A. Stemmann, W. Hansen; J. Cryst. Growth 311 (2009) 1839

[16]   Ch. Heyn; Phys. Rev. B 83 (2011) 165302

[17]   Zh. M. Wang, B. L. Liang, K. A. Sablon, G. J. Salamo; Appl. Phys. Lett. 90 (2007) 113120

[18]   Ch. Heyn, A. Stemmann, A. Schramm, H. Welsch, W. Hansen, Á. Nemcsics, Appl. Phys. Lett. 90, 203105 (2007)

[19]   Heyn Ch, Stemmann A, Schramm A, Welsch H, Hansen W, Nemcsics Á. Phys. Rev. B 2007; 76: 075317

[20]   M. Kalft, G. Comsa, T. Michely; Phys. Rev. B 81, 1255 (1998)

[21]   P. B. Barna; Proc. of Int. Summer School on Diagnostics and Application of Thin Films, Chulum u Trebone, Czechoslovakia (1991) pp. 295-310

[22]   P. B. Barna, F. M. Reicha; Proc. of 8th Int. Vac. Congr., Cannes, France (1980) Vol. 1, pp. 165-168

[23]   C. Herring; Phys. Rev. **82**, 87 (1951)

[24]   P. Müller, R. Kern; Surf. Sci. **457**, 229 (2000)

[25]   P. Müller, R. Kern; Appl. Surf. Sci. **162-163**, 133 (2000)

[26]   P. Müller, R. Kern; Appl. Surf. Sci. **164**, 68 (2000)

[27]   J. J. Métois, P. Müller; Surf. Sci. **548**, 13 (2004)

[28]   M. Degawa, E. D. Williams; Surf. Sci. **595**, 87 (2005)

[29]   M. Degawa, F. Szalma, E. D. Williams; Surf. Sci. **583**, 126 (2005)

[30]   W. Ostwald; Z. Phys. Chem. 34, 495 (1900)

[31]   M. Zinke-Allmang, L. C. Feldman, S. Nakahara; Appl. Phys. Lett. 51, 975 (1987)

[32]   M. Zinke-Allmang, L. C. Feldman, W. van Saaloos; Phys. Rev. Lett. 68, 2358 (1992)

[33]   G. Z. Pan, K. N. Tu; Appl. Phys. Lett. 68, 1654 (1996)

[34]   G. R. Carlow, M. Zinke-Allmang; Phys. Rev. Lett. 78, 4601 (1997)

[35]   K. Shorlin, S. Krylov, M. Zinke-Allmang; Physica A 261, 248 (1998)

[36]   A. Raab, G. Springholz; Appl. Phys. Lett. 77, 2991 (2000)

[37]   E. Z. Luo, Q. Cai, W. F. Chung, M. S. Altman, Appl. Surf. Sci. 92, 331 (1996)

[38]   N. Kaiser, A. Cröll, F. R. Szofran, S. D. Cobb, K. W. Benz, J. Cryst. Growth 231, 448 (2001)

[39]   A. Cröll, N. Salk, F. R. Szofran, S. D. Cobb, M. Volz, J. Cryst. Growth 242, 45 (2002)

[40]   F. R. de Boer, R. Boom, W. C. M. Mattens, A. R. Midema, A. K. Niessen, Cohesion in Metals (North-Holland, New York, 1988) p. 127

[41]   Á. Budó, Experimental Physics, Vol. I. (NTK-Publ., Budapest, 1997), p. 235

[42]   X. Huang, S. Togawa, S.-I. Chung, K. Terashima, S. Kimura, J. Cryst. Growth **156**, 52 (1995)

[43]   U. König, W. Keck, J. El.chem. Soc. **130**, 685 (1983)

[44]   B. Jones, J. Chem. Phys. **41**, 3199 (1964)

[45]   R. Popescu, E. Müller, M. Wanner, D. Gerthasen, Phys. Rev B **76**, 235411 (2007)

[46]   G. A. Satukin, J. Cryst. Growth **255**, 170 (2003)

[47]   N. Eustathopoulos, B. Drevet, E. Ricci, J. Crys. Growth **191**, 268 (1998)

[48]   Nemcsics Á, Heyn Ch, Stemmann A, Schramm A, Welsch H, Hansen W. Mat. Sci. Eng. B 1999; 165: 118

[49]   SatukinGA. J. Cryst. Growth 2003; 255: 170

[50]   Nemcsics Á, Tóth L, Dobos L, Stemmann A. Microel. Reliab. 2011; 51: 927

[51]   E. Lendvay, T. Görög, V. Rakovics. J. Cryst. Growth 1985; 72: 616

[52]   Nemcsics Á, Tóth L, Dobos L, Heyn Ch, Stemmann A, Schramm A, Welsch H, Hansen W. Superlatt. Microstr. 2010; 48: 351

[53]   Jiang A, Awasthi N, Kolmogorov AN, Setyawan W, Borjesson A, Bolton K, Harutyunyan AR, Curtarolo S. Phys. Rev. B 2007; 75: 205426

[54]   Sun J, Simon SL. Therochimica Acta 2007; 463: 32

[55]   Wautelet M, Beljonne D, Brédas JL, Cornil J, Lazzaroni R, Lecère P, Alexanre M, Gillis P, Gossuin Y, Muller R, Ouakssim A, Roch A, Duviver D, Robert J, Gouttebaron R, Hecq M, Monteverde F; Nanotechnologie, Oldenbourg Verlag München, 2008